energies

MDPI

Article

Numerical Assessment of Interference Caused by Commissioning New Wells in the Shale Gas Gathering System

Na Li [1,*], Wu Liu [1], Man Chen [2], Shuang Li [2] and Yanli Luo [2]

[1] Petroleum Engineering School, Southwest Petroleum University, Chengdu 610500, China
[2] Changning Natural Gas Development Company, CNPC Chuanqing Drilling Engineering Co., Ltd., Chengdu 610056, China
* Correspondence: 15213833420@163.com

Abstract

During the development of multiple wells of shale gas, coproduction under varying pressures induces interference. High-pressure wells impose backpressure on low-pressure wells, thereby restricting overall reservoir productivity. Accurate interference characterization is critical for efficient development. This study examines 42 gathering platforms within the Changning 201 Block. A three-tier surface gathering network hydraulic model ('Platform-Gathering Station-Central Station') was established. The model calculates key node pressures in the pipeline system following the integration of new wells. Unlike conventional interference studies that primarily focus on the reservoir scale and overlook the critical role of the surface gathering pipeline network as a propagation pathway for interference, this paper, for the first time, extends interference analysis from the "reservoir–wellbore" system to the full surface pressure system encompassing "wellhead-platform-gas gathering station-central station". A transferable three-stage engineering decision-making workflow of "diagnosis-comparison-coordination" is proposed. This evaluates the extent to which the production of new wells at different development stages interferes with the pressure and productivity of existing gas wells, and enables a quantitative assessment of the influence of pressure-boosting technology on well deliverability and auxiliary measures. This research confirms that the model presents calculation errors of less than 3%. The commissioning of seven new wells with a combined capacity of 531,000 m^3/d resulted in a total output increase of 626,900 m^3/d at the central processing station; Platform CN-30 gas well deliverability decreased by 20.7%; the implementation of appropriate pressure-boosting technology was effective, enabling an average deliverability increase of 1.27×10^4 m^3/d per well, releasing the potential deliverability of the well.

Keywords: shale gas; new gas wells; pipeline network model; gas compression; well deliverability

Check for updates

Academic Editor: Alberto Maria Gambelli

Received: 15 April 2026
Revised: 10 May 2026
Accepted: 11 May 2026
Published: 13 May 2026

Copyright: © 2026 by the authors. Licensee MDPI, Basel, Switzerland. This article is an open access article distributed under the terms and conditions of the Creative Commons Attribution (CC BY) license.

1. Introduction

During the rolling development of shale gas fields, high-pressure fluid from newly drilled wells enters the surface gathering pipeline network, which can induce reverse backpressure within the pipeline system, thereby limiting the production of existing low-pressure wells. However, existing studies lack a systematic analysis and quantitative methodology for the impact mechanism of such "surface pipeline network interference", resulting in an insufficient engineering basis for the design of new-well production schedules and booster measures.

In the complex fold-thrust belt of the southern Sichuan Basin, the Changning Shale Gas Field serves as a national shale gas demonstration zone, with technically recoverable reserves surpassing 4×10^{11} m^3. Its principal development areas include the Ning 201, Ning 209, and Ning 216 well blocks, which currently yield a daily gas output of 1350×10^4 m^3. Rolling development has led to the coexistence of multiple pressure regimes within the field, resulting in a complex pressure distribution defined by the coexistence of "high-pressure new wells–medium/low-pressure mature wells–progressively depleted gathering networks". In 2024, development plans for the Changning 201 Block included the addition of 13 new wells to further enhance recovery. The simultaneous operation of wells at different production stages has created an intricate system of high- and low-pressure gas production within the block. Owing to reverse pressure transmission effects through the surface pipeline network, wellhead pressures at legacy wells become elevated, imposing deliverability constraints. Research on interference from high-pressure wells toward low-pressure production systems has significant practical implications for achieving full-lifecycle efficient development in shale gas fields [1–3].

With the continuous development of shale gas fields, some scholars have conducted extensive research on well interference and evaluated its degree in shale gas wells [4]. Depending on the research approaches and perspectives, existing studies can be mainly classified into the following categories:

(1) Interference identification studies based on field diagnostics and monitoring: directly identifying interference phenomena using field data such as downhole pressure monitoring, production logging curves, or Blasingame curves. Lu et al. [5] employed downhole pressure monitoring to assess interference from hydraulic fracturing wells to surrounding producers. On the basis of factors such as well pattern spacing and natural fractures, they calculated the spatial extent of well interference for these gas wells. Zhang et al. [6] identified the degree of gas well interference by comparing the characteristics of production logging and Blasingame curves under different well connection conditions. Wei et al. [7] analyzed two sets of target and offset wells in the Fuling Shale Gas Field. By applying rate-normalized pressure (RNP) analysis and its derivative, they assessed changes in the stimulated reservoir volume before and after fracturing treatments. On the basis of diagnostic plots derived from production logging, they identified the degree of well interference and quantified the change in the SRV values. Chen et al. [8] established a pressure detection boundary propagation model for gas wells, derived an interference identification chart, and evaluated the degree of inter-well interference using the productivity index method and the decline curve analysis method. Although the aforementioned field monitoring methods can effectively identify interference phenomena, their diagnostic criteria are primarily derived from downhole or reservoir data, making it difficult to distinguish whether the observed pressure buildup is caused by reservoir depletion or reverse backpressure propagation within the surface gathering network. Consequently, the true source of interference cannot be accurately identified.

(2) Analysis of interference mechanisms and fracture propagation based on numerical simulation. Using the embedded discrete fracture model (EDFM), reservoir numerical simulation, or complex fracture propagation models, the generation and propagation laws of interference are revealed at the mechanistic level. Zhang et al. [9] employed EDFM to characterize the fracture grid of multi-fractured horizontal wells and simulated type curves of well interference under six scenarios. Ren et al. [10] utilized reservoir numerical simulations to develop a production prediction model for multi-cluster stimulated reservoir volume fracturing in horizontal wells. They evaluated the effective stimulated area and quantified the degree of pressure depletion in surrounding wells. Heng et al. [11,12] guided by a geology-engineering integration approach, developed a numerical model

for complex fracture propagation during hydraulic fracturing in a four-well staggered pattern on a Pad Ning 209X1. The fracturing stages contributing to well interference were identified, and it was proposed that gas wells may induce interference in neighboring wells through natural fracture systems. While capable of characterizing fracture propagation and pressure depletion propagation, these numerical simulation methods generally assume free discharge of wellhead pressure, neglecting the constraining effect of the actual outlet pressure of the gathering pipeline network on gas well production, which deviates from the realistic operating conditions of multi-well shared pipeline networks.

(3) Machine learning and data-driven prediction of interference degree. Using production data combined with machine learning algorithms, predictive models for interference degree or estimated ultimate recovery (EUR) are established. Zhang et al. [13] applied the PCA algorithm to reduce the dimensionality of gas reservoir production data. On the basis of the K-means algorithm, they categorized the degree of well interference into three classes: high, medium, and low. By integrating the random forest method, they established a regression prediction model for the degree of well interference in gas wells. The prediction accuracy reached 92.07%. He et al. [14,15] proposed evaluating the well performance interference caused by hydraulic fracturing in multi-fractured horizontal wells within the WY shale gas reservoir, both before and after fracturing operations, via two metrics: the extent of gas production loss and the extent of gas production recovery. They classified the computed results into three categories and quantified the extent of their impact on shale gas well production. Niu et al. [16,17] combined four machine learning techniques—K-Nearest Neighbor (KNN), Support Vector Machine (SVM), Random Forest (RF), and Gradient Boosting Decision Tree (GBDT)—to build an EUR prediction model for gas wells, and indicated that the SVM algorithm performs as the optimal prediction model for gas well EUR. Machine learning models can rapidly predict the degree of interference; however, the "interference labels" used in training datasets often inherently incorporate the effects of surface network backpressure. preventing the models from isolating the contributions of reservoir factors from those of the pipeline network and thereby restricting their causal interpretability.

However, the aforementioned studies share a common and critical limitation: inter-well interference has largely been treated as a reservoir- or wellbore-scale issue, with primary emphasis placed on hydraulic fracture connectivity, pressure depletion propagation, well spacing optimization, and machine learning-based prediction. The role of the surface gathering network as a key pathway for interference transmission has not been considered. In fact, the gathering pipeline network in a shale gas field exhibits a "branch-loop" structure, where any pressure fluctuation at one point can propagate throughout the entire system. When new wells are commissioned, the high-pressure fluids entering the gathering system can generate reverse backpressure within the pipeline network, which acts on existing medium- and low-pressure wells. This leads to a passive increase in wellhead pressure and a reduction in production pressure differential, thereby systematically constraining the overall production potential of the block.

In this paper, this phenomenon is explicitly defined as "surface pipeline network interference": the high-pressure fluid from newly gas wells, transmitted reversely through the surface gathering pipeline network, causes pressure elevation and productivity-constraining effects on the in-service low-pressure production system. The essence of this phenomenon lies in the hydraulic coupling among gas wells operating under multiple pressure systems within the gathering network. Since different pads share the same gathering and transportation pathway, a pressure fluctuation at any node can trigger pressure redistribution throughout the entire system. This pressure-coupling mechanism fundamentally differs from conventional reservoir interference and represents an independent

engineering problem induced by hydraulic coupling within multi-pressure surface gathering facilities. To address this, this paper extends interference analysis to the full surface pressure system from wellhead to platform, gathering station, and central station, identifies network backpressure as the primary propagation pathway, proposes a three-level pressure node analysis framework (platform-gathering station-central station) to locate and quantify interference, and distills a three-stage engineering decision workflow of "diagnosis-comparison-coordination", providing a transferable management methodology for analogous shale gas fields.

Currently, researchers both domestically and internationally have investigated the technical capabilities of internationally recognized commercial multi-phase flow simulators through numerical simulations and field validation [18,19]. These studies identified PIPESIM software as an integrated platform for simulating and optimizing the design of reservoir, wellbore, and surface pipeline network systems. It is particularly well suited for modeling and simulation of large-scale complex gas-liquid mixed transport pipeline networks. Shi et al. [20] utilized PIPESIM software to establish wellbore models and pipeline network topology models for 40 gas wells in the NH201 block. They calibrated the models using the Beggs–Brill revised (BBR) algorithm, achieving model fit accuracy with field production data that met engineering application standards. Li et al. [21,22] addressed the characteristics of Yan'an Gas Field's multi-stage gathering system and employed PIPESIM and TGNET software to construct gathering pipeline models. Based on comparative analysis, PIPESIM demonstrated better consistency in predicting pressure drop for gathering/production pipelines.

Leveraging PIPESIM's significant advantages in modeling versatility and computational precision, this study uses PIPESIM version 2022.2 to establish a surface gathering pipeline network model for 42 well pads in the Changning 201 well block. The degree of surface interference is evaluated using three quantifiable indicators: (1) the percentage increase in delivery pressure at existing platforms; (2) the pressure redistribution at key nodes within the pipeline network; and (3) the absolute loss in gas production from existing platforms. The interference of new wells on system pressure at different production stages is analyzed. Based on these analyses, optimal compression deployment schemes are evaluated, and the synergistic effects of compression and auxiliary production-enhancement measures on gas well productivity are further investigated. Variations in key node pressures and pipeline pressure losses are analyzed under different flowline arrival pressures at the gathering stations.

2. Model Establishment

2.1. Basic Field Data

The Changning 201 well block gathering system comprises one central processing station, 17 compressor units, 42 well pads, and 49 gathering pipelines, forming a loop network configuration. The pipeline network topology and pipeline parameters are shown in Figure 1. Pad numbers include well counts in parentheses, red denotes producing pads, and blue denotes pads under construction. Each pipeline is annotated with elevation above sea level (unit: meter, e.g., "H: 420 m") to reflect topographic variations. The nominal diameters (DN) of certain pipelines are indicated in the figure (e.g., "DN200"), and the data are sourced from the field design drawings and as built documentation of the Changning 201 well block. The model incorporates pipeline terrain undulation, incorporating 17,640 mileage and elevation data points for all pipelines. The pipe diameter and roughness were set accordingly. The rated power (R.P) of the compressor is displayed. The detailed elevation profile of the main line from the Changning H19 gas gathering

station (G.S.)-Central Station (C.S.) is shown in Figure 2, illustrating the topographic relief characteristics considered in the pipeline pressure drop calculation.

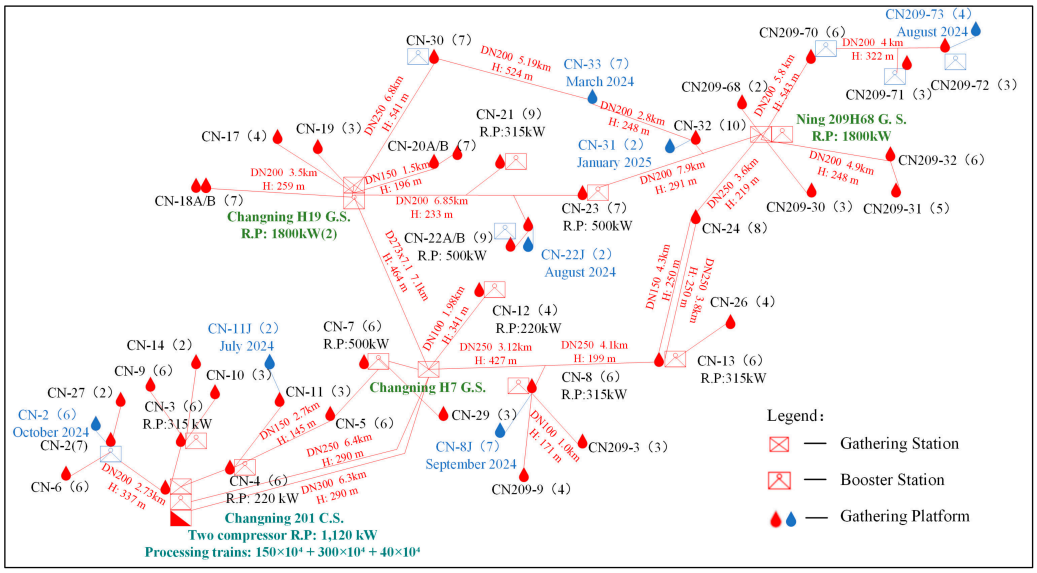

Figure 1. Pipeline network layout of the Changning 201 well block.

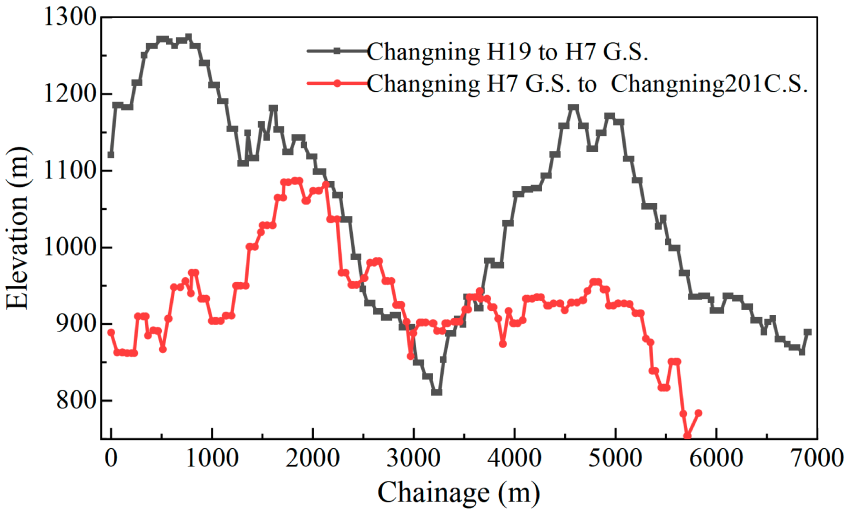

Figure 2. Pipeline mileage and elevation profile: Stations H19 to H7.

The mole fractions of gas components listed in Table 1 are determined based on field sampling and compositional analysis. The physical property parameters of each component, including critical temperature, critical pressure, and acentric factor, are automatically retrieved from the Multiflash property database embedded in the PIPESIM software. The Peng-Robinson (PR) equation of state is selected for vapor-liquid equilibrium and property calculations, as this equation has broad applicability and high accuracy in gathering pipeline network simulations. Production data such as gas production and temperature for each gathering platform are provided in Table 2.

Under the constraint of a 3.68 MPa discharge pressure in the well block pipeline network system, after injecting gas volume from the new CN-33 platform, the downstream processing station's delivery capacity failed to increase correspondingly. This causes pressure waves to propagate upstream, resulting in backpressure at gathering platforms remote from booster stations. As the production pressure differential narrows and the

wellhead pressure increases, the development of gas well productivity in the Changning 201 block will be constrained.

Table 1. Gas composition of the Changning 201 well block.

Name	Mole Fraction (%)	Name	Mole Fraction (%)
Water	1.477672	Hydrogen	0.000985
Methane	97.25547	Helium	0.018717
Ethane	0.553635	Nitrogen	0.235443
Propane	0.009851	Oxygen	0.010836
Carbon Dioxide	0.437391		

Mole Fraction: the percentage of that component's amount relative to the total.

Table 2. Gathering platform production data.

Platform Name	Gas Production Rate (m^3/d)	Water Production Rate (m^3/d)	Temperature (°C)	Delivery Pressure (MPa)	Platform Name	Gas Production Rate (m^3/d)	Water Production Rate (m^3/d)	Temperature (°C)	Delivery Pressure (MPa)
CN-18	81,457	8	22	1.59	CN-30	663,450	71.16	20	4.54
CN-17	4536	2	21	1.58	CN-32	341,909	17	20	2.95
CN-19	53,116	3	22	1.34	CN-3	96,797	11	20	1.57
CN-20	111,434	9	22	1.79	CN-6	90,850	7	22	1.64
CN-21	159,709	15	20	1.62	CN-7	24,220	6	14	3.80
CN-22	95,349	8	20	1.86	CN-9	74,205	6	19	1.66
CN-23	78,735	6	19	1.58	CN-12	52,629	4	14	3.93
CN209-3	12,813	1	20	1.60	CN209-9	153,800	4	20	1.72
CN209-30	106,094	6	20	4.98	CN-14	23,565	3	22	1.85
CN209-31	231,318	21	20	5.14	CN-2	25,399	7	23	1.60
CN209-32	152,605	18	21	5.0	CN-24	105,689	7	22	1.61
CN209-68	93,194	3	20	4.95	CN-26	57,034	3	19	1.52
CN209-70	245,532	19	22	5.32	CN-27	40,379	3	21	1.56
CN209-71	94,766	12	21	5.30	CN-29	38,271	3	20	4.04
CN-8	28,700	3.7	23	5.35	CN-13	62,301	6	21	5.01

2.2. Surface Gathering Pipeline Network Simulation Model

Using PIPESIM software as the primary research tool, the key steps for constructing the pipeline network model are as follows:

① Define the gas composition and PVT properties for each gathering well pad;

② Input temperature and gas production rates per pad based on actual operational data;

③ Set inlet/outlet boundary conditions for the well block pipeline network;

④ Set pipeline specifications (diameter, mileage, elevation profile, wall thickness, and roughness, etc.);

⑤ Establish a three-tier surface gathering network model structured as "well pad → gathering station → central processing station".

By accounting for pressure variations over time in the Changning 201 surface pipeline network and using daily gas production rates and temperatures at the well pads as input parameters, with the central processing station arrival pressure as the boundary condition, and installing compressors and heaters at gathering stations and well pads, a hydraulic model for the surface gathering pipeline network was established, Figure 3 shows a visualization schematic diagram of the pipeline network topology visualization.

In addition, the configuration and selection of key units in the model include the following: (1) For gathering pipelines with undulating terrain, the Beggs & Brill Revised correlation is used for calculating pressure drop and liquid holdup, effectively accounting for the impact of pipeline inclination on gas-liquid flow patterns and pressure loss; (2) For nearly vertical pipeline sections, the Hagedorn & Brown (HBR) correlation, which is more suitable for vertical flow, is applied; (3) Compressors in the model are set to operate at a fixed compression ratio, with the ratio determined based on the historical average operating

data of each unit; (4) To compare the scenarios in Section 4.2 where the production from new platforms is delivered to different boosting stations, in the model, control valves are used to switch gas flow paths, e.g., opening the valves along the path to a specific boosting point while closing alternate paths; (5) The model adopts the inlet pressure of the central station as the outlet boundary condition. As the most stable and controllable node in the gathering system, the fluid in the gathering network flows from the platforms toward the central station via the gathering stations, whereas the pressure wave propagates reversely upstream from the central station. This configuration faithfully reflects the backpressure constraint effect of downstream processing capacity on upstream production. It ensures the convergence of steady-state calculations and the complete causal chain of "central station pressure fluctuation→gathering station response→platform delivery pressure change". When the central station pressure fluctuates, the model can solve stage by stage from downstream to upstream, resulting in a clear logic and a closed loop.

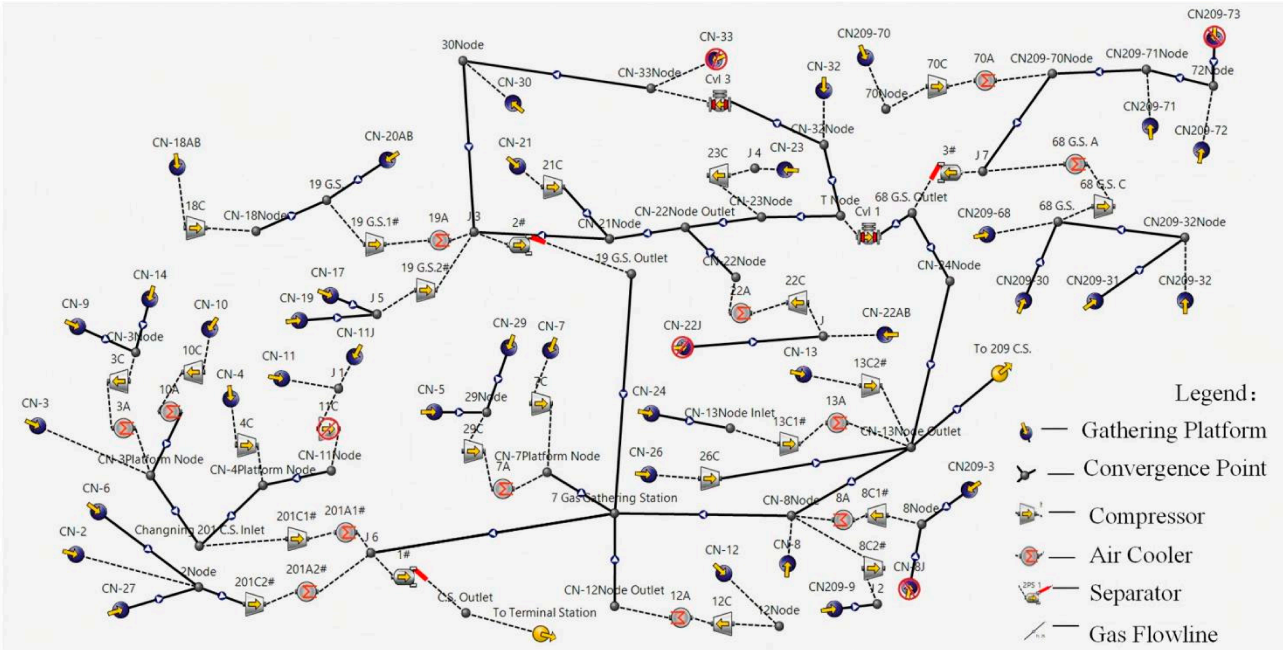

Figure 3. Changning 201 Field: Visualization Schematic of Pipeline Network Topology.

2.3. Model Assumptions and Limitations

The shale gas gathering network hydraulic model established in this study is based on the following key assumptions and limitations, and is considered most reliable within the specified scope:

(1) Steady-state assumption: The model employs PIPESIM for steady-state simulation, aiming to analyze the long-term average interference effects and trend behavior when the system reaches a new pressure equilibrium after the commissioning of new wells, rather than capturing instantaneous pressure fluctuations, water hammer effects, or complex transient liquid holdup variations induced by step changes in flow rate at the moment of commissioning. The steady-state model has limited predictive capability for transient conditions; however, this study focuses on the average impact under equilibrium conditions. Therefore, the steady-state assumption is reasonable and adequate for the objectives of this paper. The evaluation of transient peak pressures or operational risks using the steady-state model falls beyond the scope of this work, and future studies are recommended to supplement these aspects with transient simulation.

(2) Field-specific network layout: The model is constructed based on the existing pipeline layout and the measured operational parameters of the Changning 201 well block.

The conclusions, such as the severity of interference and the optimal locations for boosting, are highly dependent on the block-specific network topology, compressor configuration, and pressure-level scheme. When the model is applied to other gas fields or blocks with significantly different network configurations, recalibration and reassessment of the model's applicability are needed.

(3) Compressor control logic: In the model, compressors are treated as operating units with a fixed pressure ratio, set according to the average values derived from historical operational data. Key factors such as actual multi-compressor parallel cooperative control, surge protection, operating envelope, reliability, energy consumption, and sensitivity to gas composition and seasonal temperature variations are not considered. Under steady-state equilibrium conditions, the suction and discharge pressures of each compressor tend to stabilize; therefore, adopting a fixed pressure ratio is a reasonable engineering approximation. The core conclusions of this study regarding the comparison and selection of boosting locations primarily depend on equipment processing capacity limits and the hydraulic characteristics of the pipeline network, rather than on the precise dynamics of the pressure ratio. Consequently, the fixed-pressure-ratio assumption does not materially affect the main conclusions.

(4) Model calibration: The model was calibrated using nine sets of field data collected from December 2023 to May 2024, with relative errors less than 3%, providing high reliability for studies under the corresponding operating conditions. If significant changes in gas composition or large-scale modifications to the pipeline network occur, the model must be further updated and validated.

(5) Simplified treatment of multi-phase effects: The model calculates the average liquid holdup and pressure drop using empirical correlations, but does not simulate dynamic liquid accumulation or slug flow phenomena. The separation units at the gathering stations and the central station are simplified as ideal separators with 100% efficiency, assuming complete gas–liquid separation within each station and sufficient processing capacity to prevent the separators from forming a system bottleneck. This implies that the model does not account for operational pressure fluctuations or capacity limitations arising from variations in separator throughput or liquid load in practice.

(6) Physical properties and seasonal effects: Gas composition is fixed using the representative components listed in Table 1, and temperature is set as a constant based on the typical production data in Table 2, which is equivalent to assuming annual or seasonal average temperature conditions. Seasonal variations and fluctuations, and their potential impacts on gas properties and pipeline heat transfer are not considered in the model, this is standard practice in gathering pipeline network engineering design. The gas composition was not treated as a variable in this study because it is not directly relevant to the core issue of interference caused by new well production.

(7) Subsurface reservoir and geological factors: This study focuses only on the hydraulic behavior of the surface gathering pipeline network and does not couple with a transient reservoir model. The severity of inter-well interference is fundamentally influenced by subsurface conditions, including the degree of reservoir pressure depletion, natural fracture connectivity, well spacing, and reservoir depth. In reservoirs with shallow burial depth or high depletion degree, the same surface backpressure will lead to a more significant relative production loss. The model treats gas wells as fixed pressure/flow-rate boundary conditions; therefore, it cannot capture how different geological characteristics or depth-dependent pressure depletion gradients dynamically alter the interference intensity over time. Coupling the surface pipeline network model with reservoir numerical simulation is an important direction for future work to fully understand the subsurface–surface coupled interference mechanism.

(8) Single-case study: This study takes the Changning Block 201 as a single case, and the quantitative results (e.g., pressure elevation magnitude, production loss value) depend on the unique network topology, equipment configuration, and pressure hierarchy of this block. However, the established modeling-calibration-analysis workflow is generalizable; applying input data from a target block can readily construct an applicable model. Multi-block comparative validation is a subsequent direction of this research.

3. Mathematical Model

3.1. Empirical Formula for the Pressure Drop

PIPESIM software is employed primarily for steady-state simulation, optimization, and operational analysis of pipeline networks. Given the complexity of multiphase flow, directly solving the governing equations involves significant computational cost, uncertainty, and limited availability of precise data. To address these challenges, the software adopts empirical correlations—such as those developed by Beggs & Brill and Hagedorn & Brown—to simplify the governing equations, enabling rapid and reliable estimation of pressure drops in pipelines. The phase densities and viscosities of the gas-liquid system, calculated from gas composition using the PR equation of state, are directly incorporated into the density term and friction factor term in the pressure drop equations. The composition determines the fluid properties via the equation of state, thereby affecting the pressure drop and liquid holdup in each pipe segment. For surface gathering network models under constant production rates at gathering platforms, platform export pressures are calculated. The Beggs & Brill method [23] is particularly recommended for estimating gas-liquid two-phase pressure drops in undulating pipelines. On the basis of the steady-flow mechanical energy balance equation, the outlet pipeline pressure drop formula is [24]:

$$\frac{\mathrm{d}p}{\mathrm{d}x} = \frac{\left[H_\mathrm{l}\rho_\mathrm{l} + (1 - H_\mathrm{l})\rho_\mathrm{g}\right] g \sin\theta + \lambda_\mathrm{m} \frac{2\omega_\mathrm{m} G}{\pi d^3}}{1 - \frac{\left[H_\mathrm{l}\rho_\mathrm{l} + (1-H_\mathrm{l})\rho_\mathrm{g}\right]\omega_\mathrm{m}\omega_\mathrm{sg}}{P}} \tag{1}$$

For undulating pipe segments, liquid holdup is calculated using the Beggs & Brill correlation with the inclination correction factor ψ [25,26]:

$$H_\mathrm{l}(\theta) = \psi H_\mathrm{l}(0) \tag{2}$$

The Hagedorn & Brown method [27] is recommended for pressure drop calculations in vertical or near-vertical gas-liquid two-phase pipelines. The overall pressure drop equation is as follows [28,29]:

$$\frac{\mathrm{d}p}{\mathrm{d}z} = \rho_\mathrm{m} g + f_\mathrm{m} \frac{G_\mathrm{m}^2}{2DA^2\rho_\mathrm{m}} \tag{3}$$

The two-phase friction factor is calculated via the Jain equation [30]:

$$f_\mathrm{m} = \left[1.14 - 2\lg\left(\frac{e}{D} + \frac{21.25}{Re_\mathrm{m}^{0.9}}\right)\right]^{-2} \tag{4}$$

3.2. Model Evaluation Metrics

On the basis of the gas-liquid two-phase flow characteristics, BBR and HBR pressure drop correlations are employed to calculate key node pressures in the gathering network. The critical network parameters are fine-tuned to ensure that the model accurately represents variations in the gathering network system under different operating conditions. Model verification uses two primary evaluation metrics:

(1) Relative error (Δ): The deviation between the model-calculated pressure p_i and actual field-measured pressure p_i^0, reflecting model reliability.

$$\Delta = \frac{|p_i - p_i^0|}{p_i^0} \times 100\% \quad (5)$$

(2) Root mean square error (RMSE): A statistical measure quantifying the difference between actual pressures and model-calculated pressures. Lower RMSE values indicate higher prediction accuracy, with values approaching zero signifying superior model fit. n denotes the number of data points.

$$RMSE = \sqrt{\frac{\sum_{i=1}^{n} (p_i - p_i^o)^2}{n}} \quad (6)$$

Relative error and root mean square error are two standard metrics for assessing the accuracy of hydraulic models of pipeline networks. The relative error directly reflects the deviation between the calculated and measured pressures at an individual platform, and is typically required to be below 5% in engineering practice. RMSE, being more sensitive to large errors, evaluates the overall predictive consistency of the model across the entire network. The two metrics complement each other: Δ is used to identify whether the error at a specific platform exceeds the allowable limit, whereas RMSE is employed to judge system-level model reliability.

3.3. Model Verification

Based on the established hydraulic model of the surface gathering and transportation pipeline network in the Changning 201 Block, the measured gas production, temperatures, and inlet pressure of the central station for each platform on the corresponding dates are taken as input and boundary conditions. and the model is calibrated using platform pressure and liquid holdup volume, respectively.

(1) Platform pressure

Taking the diameter, wall thickness, length, and elevation of the 49 gathering pipelines, along with the gas production rate, temperature, and gas composition from the 42 gathering stations serving as model input parameters and the outlet pressure of the central station in the well block serving as the model boundary condition, the delivery pressures of the gathering stations were simulated and calculated by combining the BBR and HBR pressure drop calculation formulas. These calculated pressures were compared with the actual field delivery pressures. The friction factor in the selected correlation (ranging from 0.01 to 0.05) was inversely adjusted to reduce the error between the calculated and observed values, thereby improving the accuracy of the surface gathering network simulation. Taking the calibration results from 26 May 2024, as an example (Table 3), Different colors are used to annotate the values according to their magnitude (e.g., green for <1%, yellow for 1–2%, orange for 2–3%). The root mean square error (RMSE) for the pipeline network gathering stations was 0.06 MPa, with a Δ = 1.12%. This meets the requirements for field engineering applications.

Table 3. Pipeline network simulation model pressure calibration results for 26 May 2024.

Platform Name	Actual Pressure (MPa)	Calculated Pressure (MPa)	Relative Error (%)	Platform Name	Actual Pressure (MPa)	Calculated Pressure (MPa)	Relative Error (%)
CN-18	1.59	1.54	3.14	CN-30	4.54	4.56	0.44
CN-17	1.58	1.55	1.89	CN-32	2.95	2.89	2.03
CN-19	1.34	1.32	1.49	CN-3	1.57	1.59	1.27
CN-20	1.79	1.78	0.56	CN-6	1.64	1.61	1.83
CN-21	1.62	1.60	1.23	CN-7	3.80	3.72	2.11
CN-22	1.86	1.87	0.54	CN-9	1.66	1.66	0.00
CN-23	1.58	1.59	0.63	CN-12	3.93	3.94	0.25
CN209-3	1.60	1.55	3.13	CN209-9	1.72	1.68	2.33
CN209-30	4.98	4.91	1.41	CN-14	1.85	1.80	2.70
CN209-31	5.14	5.10	0.78	CN-2	1.60	1.56	2.50
CN209-32	5.0	5.01	0.20	CN-24	1.61	1.61	0.00
CN209-68	4.95	4.91	0.81	CN-26	1.52	1.53	0.66
CN209-70	5.32	5.30	0.38	CN-27	1.56	1.56	0.00
CN209-71	5.30	5.37	1.32	CN-29	4.04	4.05	0.25
CN-8	5.35	5.29	1.12	CN-13	5.01	5.05	0.80

(2) Liquid holdup volume

The pipe diameter, wall thickness, length, and elevation of 49 gathering pipelines in the network; the pressure, temperature, and gas composition of 42 gathering platforms are used as input parameters of the model; and the outlet pressure of the central station of the block is used as the boundary condition of the model. The platform liquid holdup was calculated and compared with the field-measured liquid volume. The model accuracy was improved by adjusting the friction factor or pipeline roughness. Based on the pipe material and actual field operating conditions, and with reference to relevant design codes, the engineering reasonable range of roughness is determined to be 0.01~0.05 mm. During the calibration process, different values within this range are adopted for sensitivity adjustments to minimize the model error.

The field-measured liquid production rates listed in Table 4 are taken as the daily average of routine measurements at each platform, with a metering frequency of once every two hours. Liquid production from shale gas wells fluctuates frequently due to intermittent liquid unloading and cyclic discharge of wellbore liquid loading; a single measurement cannot reflect the daily average level. Using the daily average as input smooths out instantaneous fluctuations but ignores intra-day peaks and troughs in liquid production, which is the primary cause of the minor deviations between simulated and measured values. In addition, the steady-state simulation in PIPESIM assumes that the gas-liquid two-phase flow is homogeneously mixed within the pipeline, whereas in reality, local liquid accumulation and slug flow may occur in the pipeline, leading to slight deviations in the calculated liquid holdup. Overall, the relative error is controlled within 3%, indicating that the model's prediction accuracy for liquid holdup meets the requirements for engineering applications.

According to the model calibration process, nine calibrations were performed on the major nodes of the pipeline network during the period from December 2023 to May 2024, and the results are presented in Table 5. The selection of this time period for validation is mainly based on the following reasons:

Table 4. Calibration of Liquid Holdup Volume in Pipeline Network Simulation on 26 May 2024.

Platform Name	Actual Liquid Volume (m^3/d)	Calculated Liquid Volume (m^3/d)	Relative Error	Platform Name	Actual Liquid Volume (m^3/d)	Calculated Liquid Volume (m^3/d)	Relative Error
CN-18	8	7.829	2.13%	CN-30	71.16	71.203	0.06%
CN-17	2	1.957	2.15%	CN-32	17	17.427	2.51%
CN-19	3	3.021	0.70%	CN-3	11	10.954	0.42%
CN-20	9	8.927	0.81%	CN-6	7	6.903	1.39%
CN-21	15	14.837	1.09%	CN-7	6	6.160	2.67%
CN-22	8	7.787	2.66%	CN-9	6	5.857	2.38%
CN-23	6	6.103	1.72%	CN-12	4	3.918	2.05%
CN209-3	1	0.979	2.10%	CN209-9	4	4.106	2.65%
CN209-30	6	5.932	1.13%	CN-14	3	3.041	1.36%
CN209-31	21	21.576	2.74%	CN-2	7	7.157	2.24%
CN209-32	18	17.510	2.72%	CN-24	7	7.050	0.71%
CN209-68	3	2.969	1.03%	CN-26	3	2.937	2.10%
CN209-70	19	18.759	1.27%	CN-27	3	3.005	0.17%
CN209-71	12	12.030	0.25%	CN-29	3	2.954	1.53%
CN-8	3.7	3.806	2.86%	CN-13	6	5.894	1.76%

Table 5. Platform delivery pressure verification results.

Production Date	Number of Nodes	Number of Compressor Units	Relative Error (%)	RMSE (MPa)
15 December 2023	41	15	0.10	0.08
15 January 2024	40	14	0.15	0.06
15 February 2024	43	20	0.30	0.05
15 March 2024	43	20	0.66	0.07
15 April 2024	42	18	0.80	0.05
1 May 2024	43	20	0.33	0.06
7 May 2024	43	20	0.04	0.06
15 May 2024	43	22	0.53	0.07
26 May 2024	39	16	1.12	0.06

(1) The selected period from December 2023 to May 2024 corresponds to a stage in which the Changning 201 well Block experienced the sequential commissioning of new gas wells and production ramp-up, along with multiple adjustments in the number and configuration of compressor units. This period captures the production stage with the largest fluctuations in gas production and the most pronounced changes in system pressure distribution, thus allowing for a thorough examination of the model's adaptability and robustness under different operating conditions.

(2) In this study, the interference analysis of newly added gas wells officially began in June 2024; therefore, four intensive calibrations were performed in May to ensure that the model's accuracy and reliability reached an optimal state before the interference study.

The results show that for the major nodes of the gathering pipeline network, the average RMSE is 0.06 MPa, $\Delta = 0.45\%$, and relative errors within 3%. Even under complex conditions with rapidly increasing gas production and frequent adjustments in compressor unit configurations, the model maintains stable prediction accuracy, validating its robustness and logical consistency across different production scenarios. Furthermore, the model calibration adjusted the internal pipe roughness and friction factor, and its accuracy stability was validated under multiple operating conditions, there is no statistically significant issue of data overfitting.

4. Results and Discussion

4.1. Degree of New Gas Well Interference in Gathering Network

Seven new gas wells at Platform CN-33 commenced phased commissioning on May 27, delivering production alongside Platform CN-30 to the Changning H19 G.S. Figure 4 shows the pressure and production profiles of Well #3 at CN-33 post-commission. Initial high wellhead pressures significantly impact delivery pressures across existing wells upon integration into the gathering network. Interference effects varied across different production stages. In this study, "interference" is the pressure redistribution within the surface gathering network caused by the commissioning of new wells, which negatively impacts the production, pressure, and processing capacity of existing wells. This concept encompasses three quantifiable engineering dimensions: (1) the ranked percentage increase in delivery pressure changes at key nodes; (2) the overall network pressure rise when new wells are delivering at different production stages; and (3) the production loss rate (or absolute loss) of existing wells.

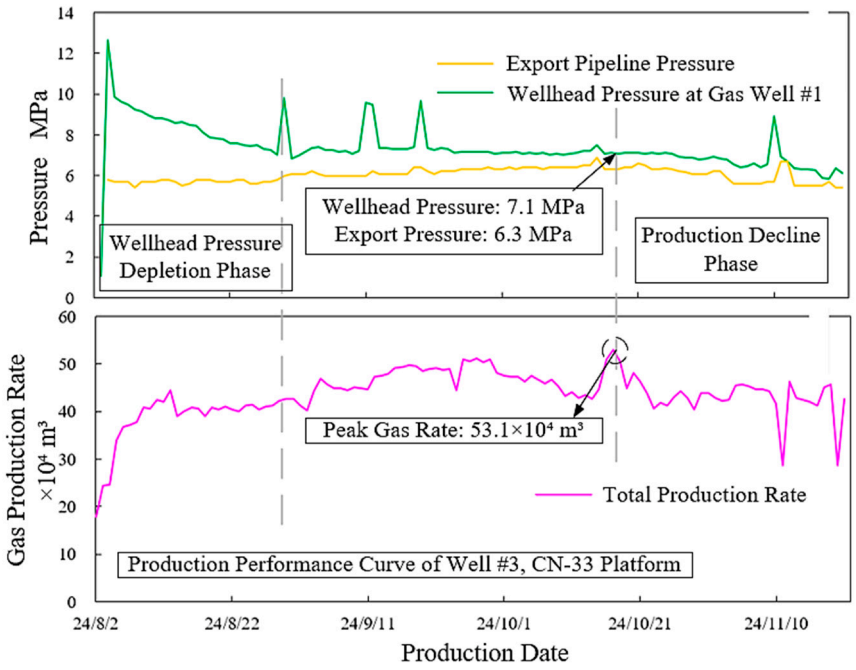

Figure 4. Well #3, CN-33 Platform: Gas Production Profile.

4.1.1. Gathering System Interference

Based on the production rates and delivery pressures of the gathering platforms without the integration of new wells or booster units and under constant production rate conditions, the Changning-201 surface gathering pipeline network model was used to calculate the delivery pressures at each platform. The analysis of pressure and production rate changes in existing wells is presented in Table 6. Three input parameters were established as boundary conditions for the CN-33 platform: ① At the start of trial production, the delivery pressure was 5.32 MPa, with a gas production rate of 1.5×10^4 m^3/d; ② After one month of operation, the delivery pressure increased to 6.5 MPa, with a gas production rate of 14.3×10^4 m^3/d; ③ After six months, upon reaching peak production, the delivery pressure was 6.3 MPa, with a gas production rate of 53.1×10^4 m^3/d.

Table 6. CN-33 Platform: Interference Severity at Varying Delivery Pressures.

Gathering Platform	Post-Commissioning Delivery Pressures (MPa)				Percentage Increase			Gas Production ($\times 10^4$ m^3/d)		Deviation ($\times 10^4$ m^3/d)
	Preceding	Trial	1 Month	6 Months	Trial	1 Month	6 Months	Preceding	Trial	
CN-30	4.56	5.01	5.32	5.44	9.7%	16.7%	19.3%	66.3	63.8	−2.5
CN-19	1.32	1.34	1.35	1.37	1.5%	2.3%	3.8%	9.6	11.2	+1.6
CN-21	1.71	1.73	1.75	1.77	1.2%	2.3%	3.5%	15.9	17.4	+1.4
CN-23	1.78	1.80	1.82	1.84	1.1%	2.2%	3.4%	7.9	7.7	−0.12
CN-20	1.79	1.81	1.83	1.84	1.1%	2.2%	2.8%	11.1	11.7	+0.53
CN-22	1.78	1.80	1.81	1.84	1.1%	1.7%	3.4%	9.5	9.3	−0.21
CN-32	2.91	2.94	2.97	2.93	1.0%	2.1%	0.7%	34.2	33.8	−0.41
G.S. Name	Preceding (MPa)		Trial (MPa)		1 Month (MPa)			6 Months (MPa)		Percentage
Changning H19	4.32		4.41		4.44			4.48		2.1%
Ning 209 H68	4.89		4.93		4.95			4.92		0.5%
Changning H7	3.69		3.71		3.74			3.70		0.8%
Central Station Aggregate Production (m^3/d)										
Changning 201C.S.	226 × 10^4		235.7 × 10^4		242 × 10^4			288.69 × 10^4		

Based on a steady-state model, the production rates of active platforms are fixed, with the outlet pressure of the central station set at 3.68 MPa, and the CN-33 platform inputs set according to the actual commissioning sequence and production rates as boundary conditions. The delivery pressures and gas production rates at the CN-33 platform exhibited significant fluctuations across different production phases, resulting in varying degrees of interference with adjacent platforms (Figure 5). Connected to the CN-30 platform via the H19 G.S. for transport to the central processing facility, the overall output at the Changning 201 C.S. increased by 62.69 × 10^4 m^3/d. When CN-33 reached its peak output of 53.1 × 10^4 m^3/d, when the export pressure increased by 18%, the delivery pressure at the gathering station rose by 0.16 MPa, with the maximum percentage increase being 2.1%. This caused higher interference levels at platforms closer to the gathering station with larger production rates, whereas platforms farther away with smaller production rates experienced lower interference levels.

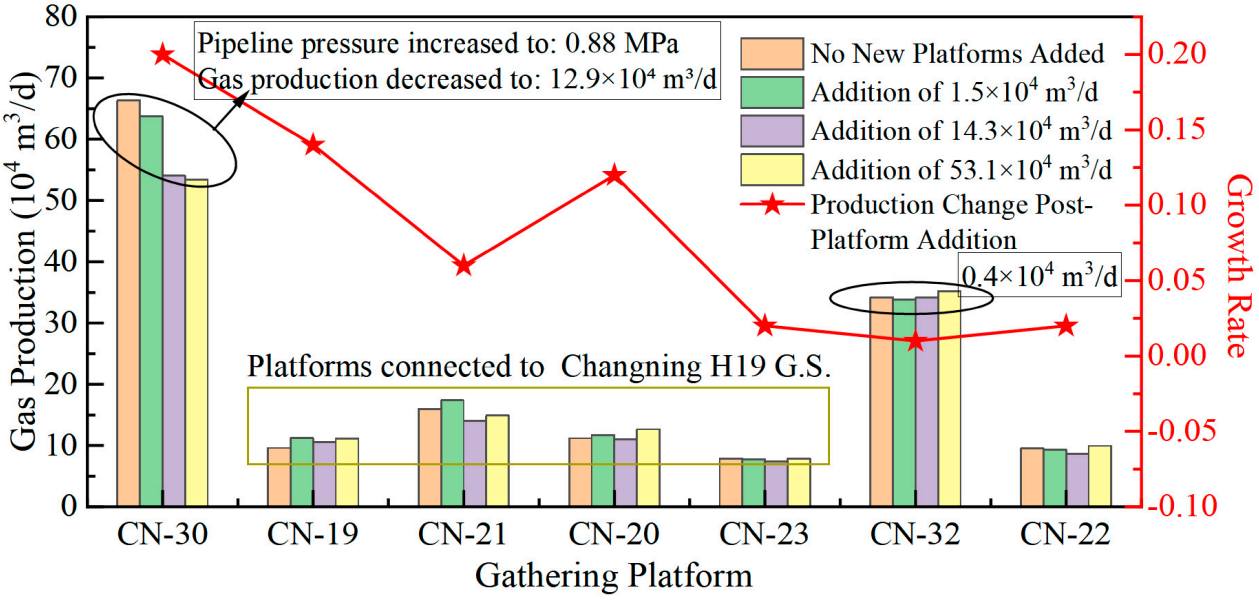

Figure 5. Platforms Impacted by Interference: Changes in Gas Production.

The CN-30 platform and the CN-33 platform share the export pipeline of the H19 G.S. The backpressure acts on the pipeline sections under the jurisdiction of this station. Moreover, the gas production rate of the CN-30 platform is as high as 66.3×10^4 m^3/d, and under high-flow-rate conditions, the frictional resistance in the pipeline section becomes more sensitive to pressure changes. Consequently, the CN-30 platform experiences the most significant interference (19.3% increase in delivery pressure and 20.7% production loss rate), demonstrating that surface pressure interference has a direct engineering economic impact. Other platforms connected to the H19 G.S. are equipped with booster compressors, which provide a buffering effect against upstream pressure fluctuations; thus, their pressure increases are controlled within 3.4%. This indicates that the sharing nodes in the network topology and the distribution of existing boosting facilities are key factors determining the distribution of interference severity. In contrast, the CN-32 platform, located relatively far from the newly commissioned wells, exhibits a total production decline of 0.4×10^4 m^3/d, corresponding to an impact of 0.7%.

The simulation results indicate that integration of newly commissioned wells into a shale gas gathering network increases the transmission pressure at existing gathering platforms within the well block, and the resulting backpressure effect leads to a decline in gas well productivity. Platforms located closer to the newly connected wells experience more pronounced pressure increases, indicating that network interference does not propagate uniformly throughout the system but instead attenuates along the shared pipeline segments. High-production platforms in close proximity to the new wells are therefore the primary recipients of interference. In contrast, platforms located farther from the newly connected wells exhibit only marginal increases in transmission pressure. Furthermore, once the new wells are connected to the gas gathering station, variations in transmission pressure can also occur at the platforms under the jurisdiction of that station. From an engineering perspective, preventive compression measures should be preferentially implemented at nearby high-production platforms to mitigate the propagation of reverse backpressure within the network.

In addition, the model calibration results demonstrate that the established hydraulic model possesses high predictive accuracy. The key interference indicators calculated in this study closely match field observations and can realistically characterize the degree of interference imposed by newly commissioned wells on the gathering network system. Therefore, the quantitative results can be directly applied to support engineering decision-making.

4.1.2. CN-30 Platform Interference from New Wells

The seven gas wells at Platform CN-33 were commissioned in a staggered manner, resulting in varying degrees of interference within the gathering system after integration. The pressures and production rates of the seven new wells at different commissioning stages were set as model input conditions. The analysis revealed that the most severe interference occurred at Platform CN-30. Figure 6a,b demonstrate the pressure and production impacts on Platform H30 from sequential well commissioning. (1) Well #3 at Platform CN-33 commenced production on 27 May 2024. As of 1 August, all seven wells were operational. The delivery pressure at Platform CN-30 increased by 1.14 MPa, the fundamental reason for this pronounced pressure rise is that CN-30 and CN-33 share the same export pipeline of the H19 G.S.; after the high-pressure fluid from the new well is injected, reverse backpressure acts directly on the CN-30 platform through the common pipeline segment. The average wellhead pressure increased by 0.47 MPa. The total gas production decreased from 63.76×10^4 m^3/d to 56.13×10^4 m^3/d. (2) After the CN-33 platform gas wells were fully put into production, the maximum deliverability was 17.97×10^4 m^3/d at an export pressure of 6.2 MPa. When gas was exported simultaneously with the CN-30 platform,

the production loss reached 13.2 × 10^4 m^3/d. This indicates that the initial moderate pressure rise has a relatively mild impact on production; however, once a certain threshold is exceeded, the production pressure differential shrinks sharply, and production exhibits an accelerating decline trend.

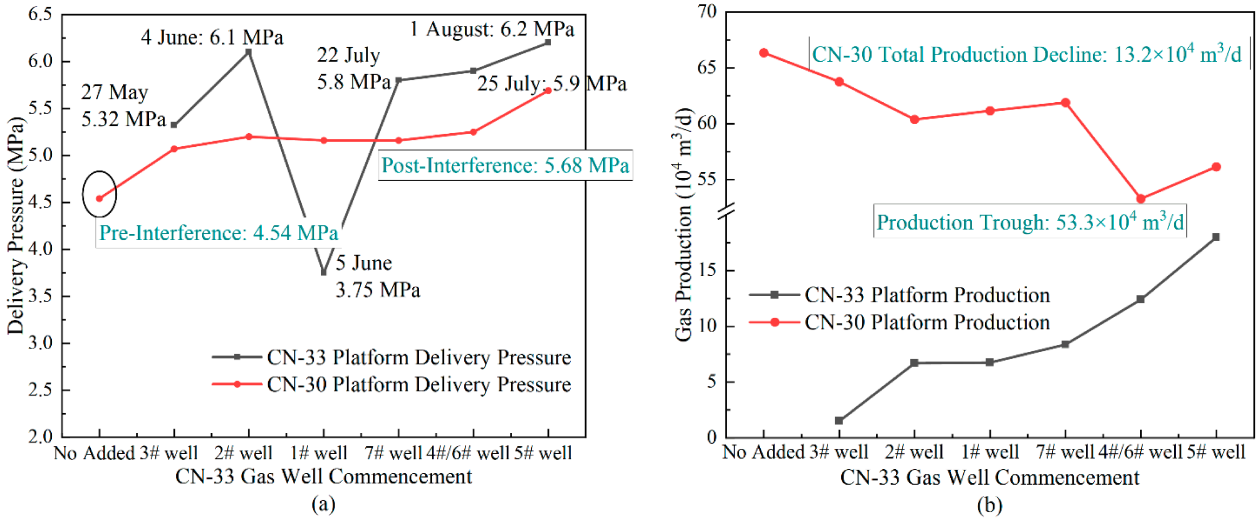

Figure 6. CN-30 Platform: Interference Severity on Delivery Pressure (**a**) and Production Rate (**b**).

Therefore, during the development of new production capacity in the gas field, the sub-optimal integration approach for newly added capacity resulted in a reduction in existing platform production that was nearly equivalent to the scale of the newly added capacity. Additionally, the phased commissioning of new gas wells subjects critical nodes in the gathering system to recurrent pressure surges, necessitating frequent adjustments to operating parameters and compression strategies. The following measures are recommended:

① Simultaneous production start-up of gas wells at the CN-33 platform should be implemented, which can significantly reduce the frequency of disturbances at critical nodes of the pipeline network, thereby enhancing overall operational stability and controllability.

② Implementing boosting technology in advance at the CN-30 platform constitutes a proactive intervention before the production pressure differential disappears, thereby avoiding a vicious cycle of "low pressure → shut-in" and maximizing the productivity development of the gas field.

Figure 7 shows the wellhead pressure (W.P.) and delivery pressure (D.P.) trends for gas wells under the CN-30 platform. Well #1 commenced initial production testing and commissioning on 10 October 2023, with output directed to the Changning H19 Gas Gathering Station for delivery. As of 10 April 2024, the wellhead pressure had declined from 9.5 MPa to 7 MPa, with a current production rate of 10.3 × 10^4 m^3/d. Owing to the commission of new gas wells, intermittent production commenced in all the wells in June as the wellhead pressures approached the platform delivery pressure. To mitigate this, pressure-boosting measures were deployed in advance across the wells in July. Post-compression, the deliverability of Well #1 increased from 5.29 × 10^4 m^3/d to 10.47 × 10^4 m^3/d. Well #2 achieved a 3.16 MPa differential pressure between the wellhead pressure and delivery pressure, yielding a deliverability of 10.31 × 10^4 m^3/d. The total well deliverability increased by 33.05 × 10^4 m^3/d, and the production enhancement efficiency reached 87.4% (Figure 8).

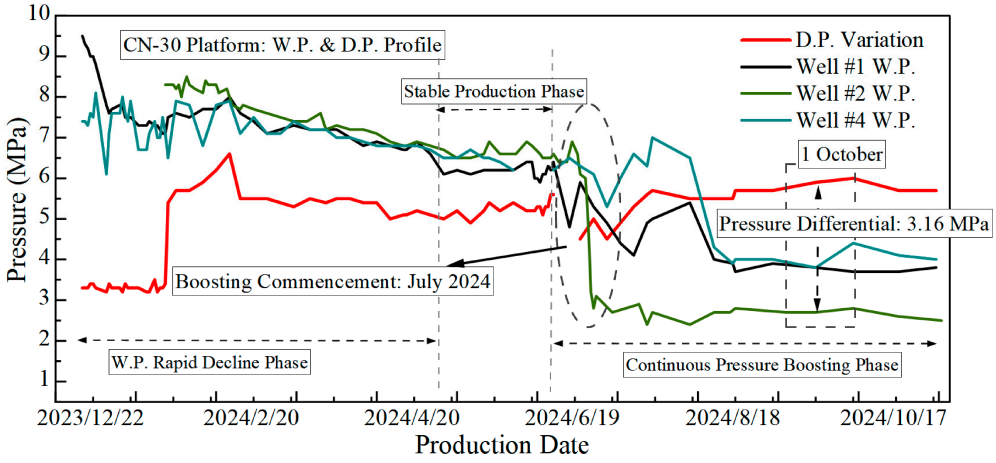

Figure 7. CN-30 Platform: Boosting Timing Optimization.

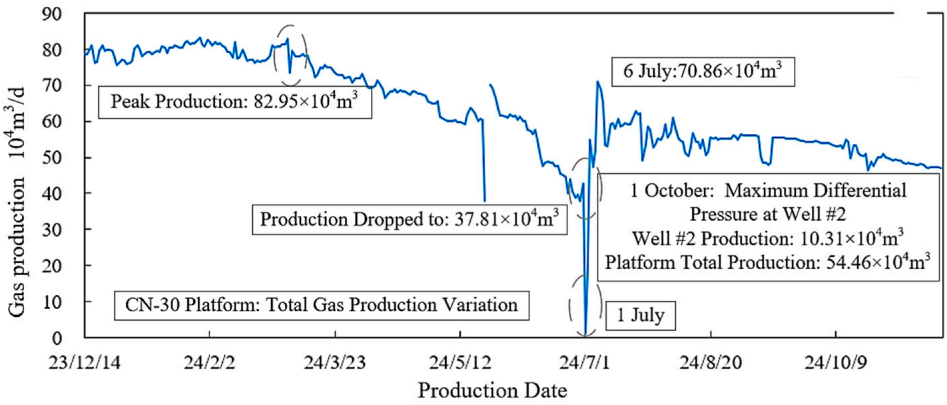

Figure 8. CN-30 Platform: Total gas production profile.

4.2. Pressure-Boosting Location Comparative Selection for New Platform Integration

As of the end of October 2024, the pressure differential between the wellhead pressure of the gas wells on the CN-33 platform and the export pipeline pressure gradually approached 0. The pressure-boosting measures were initiated in November. However, the choice of booster location is limited by the equipment capacity of the existing gathering system. Based on the topology of the gathering and transportation pipeline network in the Changning 201 well block, the booster stations in close proximity to the CN-33 platform include the CN-30 platform booster station and the Ning 209H68 G.S. booster station. A comparative analysis is conducted for these two booster station locations (Figure 9):

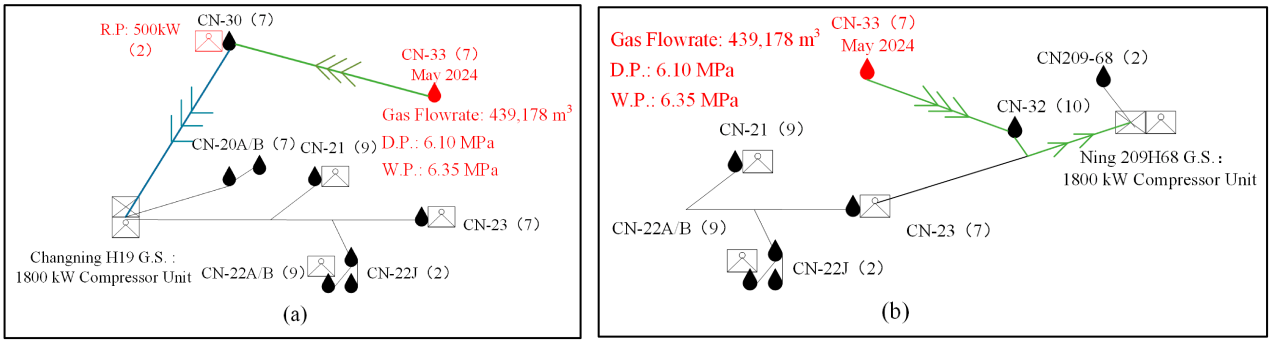

Figure 9. CN-33 Platform: boosting location option comparison. (**a**) installing a new compressor at the H30 platform; (**b**) routing high-pressure gas via the CN-32 platform to the compressor at the Ning 209H68 G.S.

(a) Install a new 500 kW reciprocating compressor at the H30 platform. The gas from the CN-33 platform is compressed by the compressor at the CN-30 platform before it gathers at the H19 G.S. for export.

(b) High-pressure gas from the CN-33 platform flows to the CN-32 platform and then enters the 1800 kW compressor at the Ning 209H68 G.S. via the pipeline connecting the CN-32 platform through a 'T-junction connection'.

On the basis of the hydraulic model of the surface gathering pipeline network in the Changning 201 well block, gas flow from the CN-33 platform was routed to different compression points by regulating control valves. As shown in Figure 10:

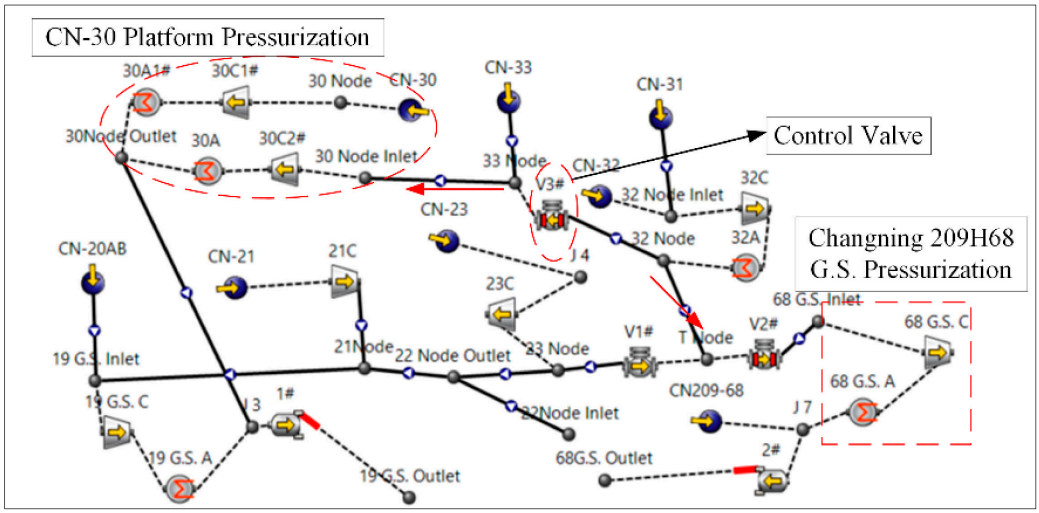

Figure 10. Boosting location simulation schematic.

(1) When the gas flow from the CN-33 platform is directed to Compressor No. 2 at the CN-30 platform for compression, the calculated compressor load reaches 93.2%, which remains within the acceptable range. The compression unit's processing capacity exceeds 51.4×10^4 m^3/d. The gathered gas volume at the H19 gas gathering station ranges from 77.95×10^4 m^3/d to 143.95×10^4 m^3/d. The Changning H19 G.S. compressor has a capacity of 145.8×10^4 m^3/d (suction pressure: 2.0 MPa, discharge pressure: 5.5 MPa). The compression capacity satisfies the pressure-boosting requirements of the gathering station. Within the limits of the existing equipment capacity, the wellhead pressure at the CN-33 platform can be effectively reduced, thereby releasing production capacity.

(2) When routing the gas flow from the CN-33 platform to the H68 G.S. for compression, the station compressor (with a processing capacity of 73.4×10^4 m^3/d at a suction pressure of 2.0 MPa/discharge pressure of 5.0 MPa) experiences overload conditions (load exceeds 100%), and the equipment capacity constraint is activated. This caused the wellhead pressure to increase and the production rate to decrease at other low-pressure platforms that share the same compression system. Consequently, the full production potential of the gas field was constrained, confirming that the Ning 209H68 G.S. lacks sufficient compression capacity for the CN-33 platform gas volume.

The selection of the pressure-boosting location is a problem of hydraulic rebalancing of the pipeline network under equipment capacity constraints. The feasibility of Scheme (1) lies in the fact that the redundant processing capacity of the existing compressor at the CN-30 platform can accommodate the incremental gas volume, and the additional load does not trigger the equipment bottleneck of the H19 G.S. In contrast, Scheme (2) fails because the additional gas volume exceeds the processing capacity limit of the compressors at the H68 G.S. Under overload conditions, the compressors are unable to provide effective pressure boosting; overloading not only fails to achieve effective boosting but also transmits

backpressure through the gathering station header to other low-pressure gas wells within the station, resulting in a negative chain effect of "boosting at one point while suppressing multiple others." Therefore, in actual operation, priority should be given to evaluating the load margin of existing compressors rather than considering only their spatial location.

Additionally, the installation cost for one 500 kW reciprocating compressor falls within the range of (1.65–2.63) million RMB, whereas the power distribution system cost for an 1800 kW compressor ranges from (1.5–2.5) million RMB. This represents a 70% reduction in cost by comparison. Therefore, based on the pipeline network topology, equipment capacity, and economic considerations for the Changning 201 well block, and under the premise of avoiding the activation of system bottlenecks, constructing a new boosting station at the CN-30 platform to boost the CN-33 platform is recommended. Based on cost comparison and production enhancement effects, the recommended scheme exhibits clear economic feasibility.

4.3. Impact Study of Pressure-Boosting Technology on Gas Well Performance

4.3.1. Impact of Foam Drainage Technology on Gas Wells

Based on the production trends observed at Platform CN-33 in Figure 5, pressure boosting was implemented in November 2024 to stabilize production during the plateau development phase. In the late production stage, the decreased bottomhole flow pressure and excessive liquid loading led to unstable intermittent production. By late April 2025, hybrid foam lift + pressure-boosting technology was initiated where the foaming agent converts wellbore liquids into low-density foam to reduce the hydrostatic backpressure. In contrast, compression lowered the wellhead pressure to increase the lifting pressure differential. This synergistic approach enhanced the liquid-carrying capacity, facilitated downhole liquid removal, and improved gas well productivity. For Well #4 (an upper dip horizontal well at Platform CN-33), the post-stimulation data in Figure 11 demonstrate a wellhead pressure reduction of 1.97 MPa and a decrease in the wellhead pressure of 0.8 MPa. The single-well productivity increases, reaching 6.63 × 10^4 m^3/d, with liquid production recorded at 12 m^3. This indicates that foam drainage effectively mitigates liquid loading within the wellbore, whereas compression alleviates backpressure within the gathering network. Through the synergistic application of these two measures, the production pressure differential is simultaneously enhanced. As a result, flow resistance is reduced throughout the entire production pathway-from the bottomhole to the wellhead and further through the gathering network-thereby enabling a more complete release of production capacity.

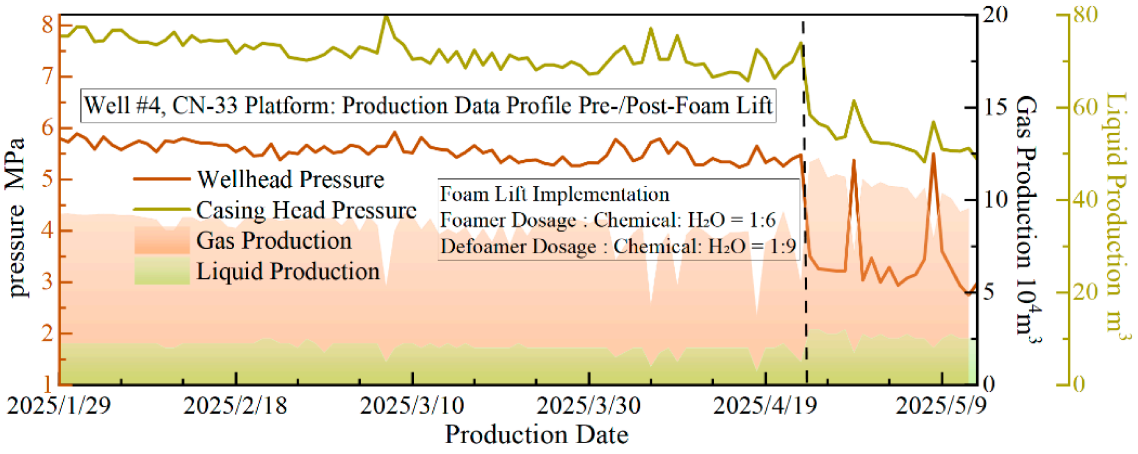

Figure 11. Well #4, CN-33 Platform: Pre/Post-Foam Lift Production Profile.

4.3.2. Influence of Plunger Lift Systems on Gas Well Performance

On 20 January 2021, plunger lift technology was implemented on four gas wells at the CN-17 platform, operating under a cycle of 120 min of shut-in followed by 180 min of production. This intermittent mode resulted in elevated initial gas flow rates when the wells were reopened, leading to pressure spikes at the wellhead and subjecting the compression equipment to shock loading. Consequently, production did not reach the expected output levels. On 21 June 2024, small-scale compression was introduced to increase pressure, subsequently evolving into an integrated production approach combining plunger lift and compression. According to the design methodology outlined in Technical Specification for Plunger Lift [31], platform compression directly reduces the wellhead pressure and average casing pressure, further decreasing the bottomhole flow pressure to increase well productivity; a reduction in the casing pressure decreases the gas volume required per lift cycle, shortens the shut-in duration for casing pressure recovery, and increases the production time, collectively improving well deliverability.

Using pre- and post-intervention wellhead pressure changes at Well #1 of the CN-17 platform as an example (Figure 12), the following observations were made. Following the implementation of pressure boosting, the flowing wellhead pressure at Well #1 decreased to 0.5 MPa, whereas the platform export pressure was maintained at 1.6 MPa. The average casing pressure decreased from 1.95 MPa to 0.92 MPa. This resulted in a reduced bottomhole flow pressure, an increased pressure differential along the wellbore, and an increase in well deliverability of 1.03×10^4 m^3. Post-compression data (Figure 13) further revealed that the plunger arrival time was reduced to 11 min upon opening the wellbore, the shake-in duration was reduced by 60 min compared with that of precompression operations, and an extended production time contributed to additional gas output.

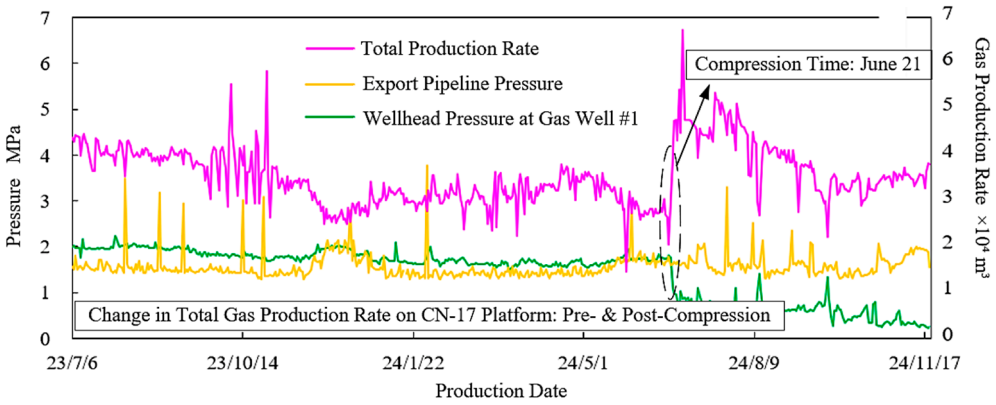

Figure 12. Well #1: Wellhead pressure and platform production changes pre/post-boosting.

4.3.3. Impact on Gas Well Deliverability

During the late-stage development of the Changning gas field, the wellhead pressure continuously decreased with production time. When the wellhead pressure approaches the delivery pipeline pressure, the number of gas wells producing intermittently increases, leading to reduced gas production rates. The implementation of pressure-boosting measures for these wells can effectively address the production constraints caused by low pressure in depleted gas wells.

For low-pressure gas wells in the late production stage, the primary function of compression is to restore the production pressure differential. Taking the CN-26 platform as an example, a screw compressor with a selected power of 220 kW and a rated discharge pressure of 3.3 MPa was installed. Table 7 presents the wellhead pressure changes before and after boosting for each gas well. After compression, the wellhead pressure decreased,

the pressure difference relative to the delivery pressure increased, and the production increased by 4.56 × 10^4 m^3/d. The boosting effect continued to strengthen three months after commissioning (total production increased to 9.48 × 10^4 m^3/d), achieving an incremental efficiency of 64.3%. These results indicate that compression not only enhances production instantaneously but also further activates reservoir deliverability by reducing bottomhole flowing pressure, thereby forming a positive feedback mechanism.

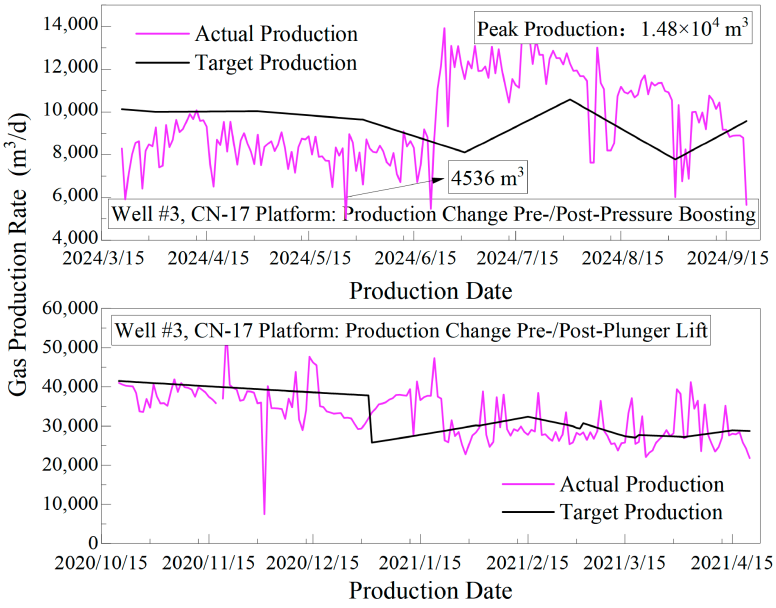

Figure 13. Well #1: Gas Production After Plunger Lifting + Boosting.

Table 7. CN-26 Platform: Pre/Post-Boosting Pressure & Total Production Changes.

D.P. (MPa)	Phase	Data Name	2#	3#	4#	5#	Aggregate Production (m^3)
1.5	Pre-compression	W.P. (MPa) Gas Production (m^3)	1.86 289	2.78 3249	1.76 3085	2.5 2898	12,122
1.3	Post-compression	W.P. (MPa) Gas Production (m^3)	1.02 18,228	3.05 16,480	0.95 20,614	1.04 2371	57,693
1.4	After 3 Months	W.P. (MPa) Gas Production (m^3)	0.92 34,384	0.8 11,343	0.8 11,807	0.9 37,251	94,785

The average single-well productivity increased by 1.14 × 10^4 m^3/d. The compressor operates at 77% load, meeting the rated power requirements. The post-compression gas production rates for all wells exceeded target production levels (Figure 14), demonstrating the maximized development of the wells' production potential.

4.4. Impact of Export Pressure on Critical Node Pressures

To investigate the influence of variations in key boundary conditions on the calculation results, a sensitivity analysis of the central station outlet pressure is conducted in this section. The export pressure at the Changning 201 Central Station was controlled within the range of (3.4~4.5) MPa, with processed gas volumes varying between (160~435.6) × 10^4 m^3/d. While meeting platform delivery requirements, existing compressor capacities were fully utilized. Numerical simulations were conducted to analyze pressure variations at critical nodes in the pipeline network. Three outlet pressure (O.P.) scenarios (3.45 MPa, 3.85 MPa, and 4.35 MPa) were modeled to calculate the pressure changes at the gathering

stations and platforms (Table 8). Under the 4.35 MPa export pressure scenario, the pressure drop variations along the trunklines are shown in Figure 15. The key findings include the following:

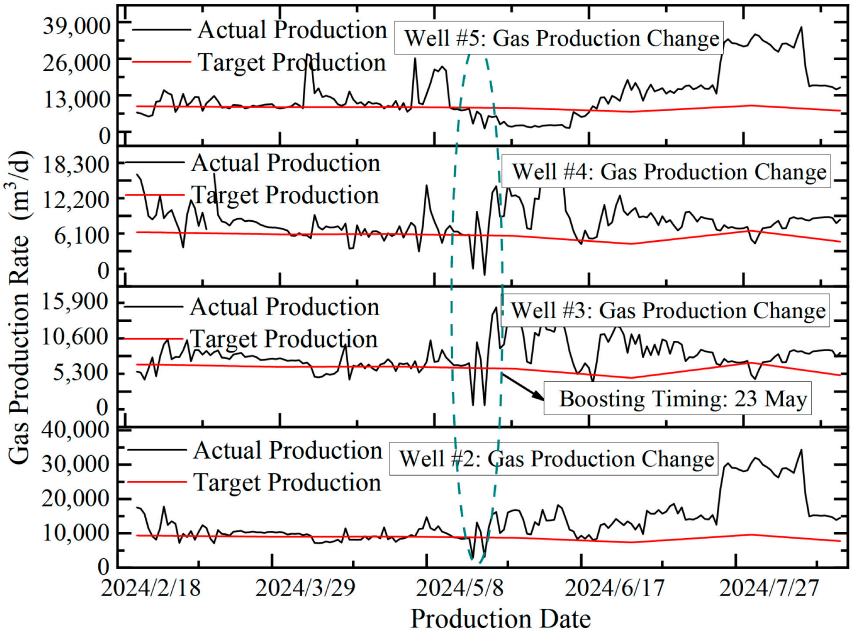

Figure 14. CN-26 Platform: Gas Production Changes Pre-/Post-Boosting.

Table 8. Key gathering stations & platforms: delivery pressure variations.

Platform Name	Production Rate (m^3/d)	Outlet Pressure 3.68 (MPa)	Outlet Pressure 3.45 (MPa)	Outlet Pressure 3.85 (MPa)	Outlet Pressure 4.35 (MPa)
7 Gathering Station	1,926,538	3.69	3.49	3.86	4.55
19 Gathering Station	1,627,897	4.34	4.15	4.48	5.06
68 Gathering Station	911,705	4.91	4.87	5.04	5.59
CN-29	38,271	4.05	3.84	4.23	4.94
CN-7	24,220	3.72	3.51	3.89	4.58
CN-2	25,399	1.54	1.46	1.61	1.80
CN-30	663,450	4.56	4.36	4.71	5.31
CN-32	152,605	2.89	2.87	2.91	2.99

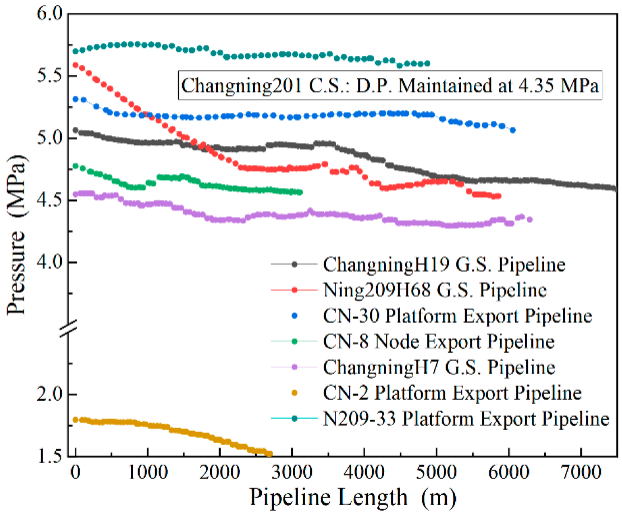

Figure 15. Platform Export Pipeline: Pressure Drop Profile.

Platforms connected to the Changning 201 C.S. via a series-compression configuration exhibited minimal pressure fluctuations, indicating the effective boosting performance of the installed compressors.

In contrast, the Changning H7 G.S., which is directly connected without compression, experienced significant pressure variations. A 0.5 MPa increase in the central station's export pressure resulted in a maximum pressure change of 0.69 MPa at H7 Station.

It can be observed that a gathering station equipped with compressor units divides the pipeline network into relatively independent upstream and downstream pressure systems. The constant pressure control at the compressor outlet effectively blocks the reverse propagation of central station pressure fluctuations to the upstream side; the platforms under its jurisdiction are minimally affected. In contrast, the H7 G.S., which has no compressor installed, is directly connected to the C.S., allowing pressure fluctuations to propagate unobstructed along the pipeline. Consequently, this station and the platforms under its jurisdiction exhibit the most pronounced changes in delivery pressure. On paths without compressor isolation, pressure waves gradually attenuate after traveling over long pipeline sections due to frictional losses; the farther from the C.S., the smaller the impact. Therefore, compressors not only provide pressure boosting, but more importantly function as "hydraulic isolators" that decouple pressure fluctuations between the upstream gathering network and the downstream processing facilities. In the design or retrofitting of gathering systems, the benefits of installing additional compressor stations along long-distance trunk pipelines extend beyond pressure enhancement itself; a more critical advantage lies in mitigating the long-range propagation of reverse backpressure within the network.

When controlling for variations in export pressure at Central Station 201, the trunkline of the CN-29 platform experiences the most significant impact (as evidenced in Figure 16). At the CN-29 platform, which is boosted and exported via the compressor-equipped H7 Gathering Station, elevated outlet pressure at H7 Station increases delivery pressures across its connected platforms. Specifically, as the Central Station 201 export pressure increased to 4.35 MPa, the platform delivery pressure increased by 0.44 MPa. Conversely, the CN-32 platform (connected via a tee connection to H19 Gathering Station but farthest from the central station) exhibited a negligible impact of only 0.02 MPa.

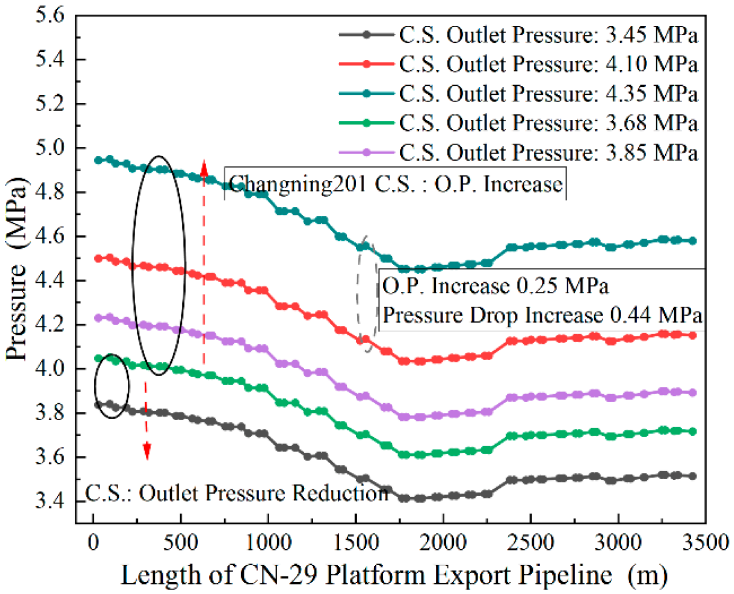

Figure 16. CN-29 Platform: Pipeline Pressure Drop.

5. Conclusions

Steady-state simulation with the commercially available software PIPESIM was performed for the key nodes in the Changning 201 block. This simulation aims to analyze the interference of pipeline network pressure and production capacity after commissioning seven new gas wells, and to investigate the impact of different development stages on the productivity of existing wells. The key findings are as follows:

(1) When the newly added gas wells on the CN-33 platform are in production at different output stages, the reverse pressure propagation through the pipeline network elevates the delivery pressure of existing wells in the well area. Platforms located close to the new wells and operating at high production rates exhibit a production loss rate of up to 20.7%, whereas wells located farther away with relatively lower production show a pressure increase of approximately 3.4%. The total gas production of the central station in the Changning 201 well area increases by 62.69×10^4 m^3/d.

(2) When new wells are diverted to gathering stations for compression and export, the wellhead pressures of other low-pressure gas wells connected to the same station become passively elevated. This pressure increase transmits downhole through the wellbore, increasing the bottomhole flow pressure and thereby constraining the deliverability. At Platform CN-30, implementing compression specifically for the CN-33 wells ensured compliance with the throughput specifications of the gathering station compressor.

(3) Implementation of the foam lift + compression process converted liquid loading into low-density foam within the wellbore, increasing the lifting pressure differential. This approach reduced both the wellhead and casing pressures while increasing the single-well productivity.

(4) After applying the plunger lift and compression process, the wellhead pressure of the gas well is reduced, which, in turn, lowers the bottomhole flowing pressure and enhances the well productivity. The production pressure differential increases to 1.1 MPa, while the average casing pressure is reduced, further lowering the bottomhole flowing pressure and enhancing gas deliverability. Additionally, the reduction in wellhead casing pressure decreases the gas volume required for a single plunger lift cycle, shortening the shut-in time by 60 min.

(5) This study proposes a three-stage engineering decision-making framework for interference mitigation, namely 'diagnosis-screening-coordination,' which has been validated through field application in the Changning 201 well block. The analytical framework is independent of specific geological conditions and can be extended to rolling development scenarios in other shale gas fields. In 'branch-loop' pipeline networks, interference intensity attenuates with distance, and platforms located near newly commissioned wells are most susceptible to production losses. Implementing "preventive compression" for existing wells expected to be affected represents a potential strategy to balance production ramp-up in new areas with stable production in mature zones. It should be emphasized that the specific numerical results reported in this paper are based on the particular conditions of the Changning 201 well block and cannot be directly extrapolated. When applied to other target blocks, the model must be recalibrated according to the specific pipeline network topology, equipment configuration, and production data of the block in question. However, the analytical methodology and the decision-making workflow themselves are generally applicable.

(6) For future research, it is recommended to couple the surface pipeline network model with reservoir numerical simulation to fully reveal the dynamic influence of subsurface factors such as reservoir pressure depletion and fracture connectivity on surface interference. For field engineering practice, strategies such as batch commissioning of new wells combined with preventive compression are suggested to shorten the interference

period and achieve a balance between production growth in new zones and stable output in mature areas. Furthermore, it is recommended that subsequent studies conduct similar analyses in more shale gas blocks to establish a comparative database of surface pipeline network interference and to validate the generalizability of the conclusions drawn in this paper.

Author Contributions: W.L.: Conceptualization, Methodology, Writing—Revised Manuscript. N.L.: Validation, Formal analysis, Writing—original draft. M.C.: Investigation, Conceptualization. S.L.: Formal analysis, Writing—original draft. Y.L.: Resources, Writing—Editing. All authors have read and agreed to the published version of the manuscript.

Funding: This work was supported by the 2023 Scientific Research and Technology Development Project "Study on Boosting Production Technology for Shale Gas Well Sites" (Grant No. 20230608-24) from Sichuan Changning Natural Gas Development Co., Ltd.

Data Availability Statement: The data that support the findings of this study are available in this article.

Conflicts of Interest: Authors Man Chen, Shuang Li, and Yanli Luo were employed by the company CNPC Chuanqing Drilling Engineering Co., Ltd., Chengdu, China. The remaining authors declare that this research was conducted in the absence of any commercial or financial relationships that could be construed as potential conflicts of interest. The authors declare that this study received funding from "Study on Boosting Production Technology for Shale Gas Well Sites" (Grant No. 20230608-24). The funder was not involved in the study design, collection, analysis, interpretation of data, the writing of this article or the decision to submit it for publication.

Nomenclature

p is the dl average pressure in the pipe segment, MPa; dl is the length of the pipe segment, m; H_l is the liquid holdup; λ is the two-phase friction factor; ρ_l is the liquid-phase density, kg/m^3; ρ_g is the gas-phase density, kg/m^3; d is the pipe internal diameter, m; ω_m is the mixture velocity, m/s; ω_{sg} is the gas superficial velocity, m/s; θ is the pipe inclination angle, °; N_{lv} is the liquid velocity number; a_4, a_5, a_6, a_7 is the flow pattern dependent coefficient; G is the mass flow rate of the mixture, kg/s; ρ_m is the mixture density, kg/m^3; D is the pipe internal diameter, m; f_m is the two-phase friction factor; G_m is the mass flow rate of the mixture, kg/s.

References

1. Hu, Y.; Yang, Y. A Comparative Study on Drag Reduction Methods for Continental Shale Drilling in the Fuxing Block, Southeastern Sichuan Basin. *Reserv. Sci.* **2026**, *2*, 81–96. [CrossRef]
2. Li, W.; Liao, J. Microscopic Analysis of Flow Resistance of Oil Displacement Fluid in Reservoir Fractures. *Reserv. Sci.* **2025**, *2*, 16–33. [CrossRef]
3. Tian, L.; Zhang, Q.; Li, X.; Li, C. Fracturing Effectiveness Evaluation Based on Flowback Data Using Pressure Transient Testing. *Reserv. Sci.* **2026**, *2*, 97–110. [CrossRef]
4. He, Y.; Guo, J.; Tang, Y.; Xu, J.; Li, Y.; Wang, Y.; Lu, Q.; Patil, S.; Rui, Z.; Sepehrnoori, K. Interwell fracturing interference evaluation of multi-well pads in shale gas reservoirs: A case study in WY Basin. In Proceedings of the SPE Annual Technical Conference and Exhibition, SPE 2020, Virtual, 11–14 October 2020. [CrossRef]
5. Lu, B.; Hu, C.F.; Ma, J. Influencing factors and countermeasures of inter-well interference of fracturing horizontal wells in Nan Chuan shale gas field. *Pet. Reserv. Eval. Dev.* **2023**, *13*, 330–339. [CrossRef]
6. Zhang, J.; Fan, H.; Yue, S.; Hu, H. Analysis of influencing factors of interwell interference in shale gas well groups and well spacing optimization. *Nat. Gas Geosci.* **2022**, *33*, 512–519. [CrossRef]
7. Pang, W.; Ehlig-Economides, C.A.; Du, J.; He, Y.; Zhang, T. Effect of well interference on shale gas well SRV interpretation. In Proceedings of the SPE Asia Pacific Unconventional Resources Conference and Exhibition, SPE 2015, Brisbane, Australia, 23–25 November 2015; p. SPE-176910-MS. [CrossRef]
8. Chen, J.Y.; Wei, Y.S.; Wang, J.L.; Yu, W.; Qi, Y.D.; Wu, J.F.; Luo, W.J. lnterwell-production interference and well spacing optimization in shale gas reservoir. *Nat. Gas Geosci.* **2021**, *32*, 931–940. [CrossRef]

9. Qing, Z. Well Interference Analysis of Shale Gas Wells Based on Embedded Discrete Fracture Model. *Geofluids* **2022**, *2022*, 1795369. [CrossRef]
10. Ren, J.W.; Bai, X.H.; Bu, J.; Wang, F.; Yu, J.Z. Analysis of influencing factors of horizontal well interwell interference and well spacing optimization in ultra-low permeability reservoir. *Unconv. Oil Gas* **2024**, *11*, 79–88. [CrossRef]
11. Heng, D.; Yang, L.X.; Peng, H.; Cai, J.S.; Gao, Y.H.; Tang, X.H.; Zhu, H.Y. Inter-well interference mechanism of complex hydraulic fractures on Ning 209X1 cube development platform. *Sci. Technol. Eng.* **2023**, *23*, 3712–3722. [CrossRef]
12. Wang, M.; Zhang, X.; Wang, H.; Hui, G.; Chen, S. Integrating geological model via A multimodal machine learning approach in shale gas production forecast. *Gas Sci. Eng.* **2025**, *139*, 205617. [CrossRef]
13. Zhang, Q.; He, F.; He, Y.W. Well interference evaluation and prediction of shale gas wells based on machine learning. *Pet. Reserv. Eval. Dev.* **2022**, *12*, 487–495. [CrossRef]
14. He, Y.; He, Z.; Tang, Y.; Xu, Y.; Xu, J.; Li, J.; Sepehrnoori, K. Interwell fracturing interference evaluation in shale gas reservoirs. *Geoenergy Sci. Eng.* **2023**, *231*, 212337. [CrossRef]
15. Zeng, B.; Chen, L.; Zhang, Z.; Sun, Q.; Zhu, H.; Tang, X.; Wang, C. Well-Interference Characteristics of the Production of Shale Well Pads: A Case in the Southern Sichuan Basin. *Energies* **2024**, *17*, 6068. [CrossRef]
16. Niu, W.; Lu, J.; Sun, Y. Development of shale gas production prediction models based on machine learning using early data. *Energy Rep.* **2022**, *8*, 1229–1237. [CrossRef]
17. Viet, N.; Hyundon, S.; Zhuoheng, C. Deep neural network model for estimating montney shale gas production using reservoir, geomechanics, and hydraulic fracture treatment parameters. *Gas Sci. Eng.* **2023**, *120*, 205161. [CrossRef]
18. Biyanto, T.R.; Umam, S.; Permatasari, K.A.; Irawan, S.; Perkasa, F.; Bayuaji, R. Gas Mass Flow Rate Optimization On Multi Gas Well System Using PIPESIM Software. In Proceedings of the ICIPEG 2016, Kuala Lumpur, Malaysia, 15 August 2016.
19. Shi, W.; Zhang, C.; Jiang, S.; Liao, Y.; Shi, Y.; Feng, A.; Young, S. Study on pressure-boosting stimulation technology in shale gas horizontal wells in the Fuling shale gas field. *Energy* **2022**, *254*, 124364. [CrossRef]
20. Shi, L.X. Optimization of NH Gathering System Based on PIPESIM Software. *Chem. Eng. Des. Commun.* **2024**, *50*, 135–137.
21. Li, C.J.; Chen, Y.X.; Mu, Y.; Song, Z.Y. Comparative Analysis of Medium and Low-Pressure Gathering Calculation Software in Yan'an Gas Field. *Pipeline Tech. Equip.* **2024**, *21*, 31–34.
22. Tian, F.B.; Wei, Y.H. Application and Differences of PIPESIM and SPS Software in Oil Pipeline Calculation. *China Pet. Petrochem.* **2016**, *16*, 73–74.
23. Beggs, H.D.; Brill, J.P. A Study of Two-Phase Flow in Inclined Pipes. *J. Pet. Technol.* **1973**, *25*, 607–617. [CrossRef]
24. Luo, S.; Jiang, H.Y.; Yao, A.L.; Jiang, W.; Zeng, Y.H. Analysis of oil field hydraulic gathering and transportation radius based on Beggs & Brill model. *Nat. Gas Pet.* **2016**, *34*, 26–29. [CrossRef]
25. Huang, Y.; Li, X.; Liu, X.; Zhai, Y.; Fang, F.; Guo, W.; Qian, C.; Han, L.; Cui, Y.; Jia, Y. Review of the productivity evaluation methods for shale gas wells. *J. Pet. Explor. Prod. Technol.* **2024**, *14*, 25–39. [CrossRef]
26. Kim, S.; Kim, W.T.; Hong, Y.; Kim, J.; Jeong, H. Enhancing pressure gradient prediction in multi-phase flow through diverse well geometries of North American shale gas fields using deep learning. *Energy* **2024**, *290*, 130291. [CrossRef]
27. Hagedorn, A.R.; Brown, K.E. Experimental Study of Pressure Gradients Occurring During Continuous Two-Phase Flow in Small-Diameter Vertical Conduits. *J. Pet. Technol.* **1965**, *17*, 475–484. [CrossRef]
28. Chen, D.C.; Xu, Y.X.; Meng, H.X.; Peng, G.Q.; Zhou, Z.F. Evaluation and Optimization of Gas-Liquid Two-Phase Flow Pressure Drop Calculation Models in Gas Wells. *Fault-Block Oil Gas Field* **2017**, *24*, 840–843. Available online: https://www.cnki.com.cn/Article/CJFDTOTAL-DKYT201706027.htm (accessed on 5 April 2026).
29. Tian, Y. Experimental and Modeling Study on Drainage Gas Recovery by Velocity String. Master's Thesis, Southwest Petroleum University, Chengdu, China, 2015.
30. Jain, A.K. Accurate explicit equation for friction factor. *J. Hydraul. Div.* **1976**, *102*, 674–677. [CrossRef]
31. National Energy Administration. *Technical Specification for Plunger Lift: SY/T 7623-2021*; National Energy Administration: Beijing, China, 2021. Available online: https://www.antpedia.com/standard/1012718343-1.html (accessed on 5 April 2026).

Disclaimer/Publisher's Note: The statements, opinions and data contained in all publications are solely those of the individual author(s) and contributor(s) and not of MDPI and/or the editor(s). MDPI and/or the editor(s) disclaim responsibility for any injury to people or property resulting from any ideas, methods, instructions or products referred to in the content.